THE PLANE TURBULENT WALL JET
PART I. JET DEVELOPMENT AND FRICTION FACTOR

BY

G. E. MYERS, J. J. SCHAUER, AND R. H. EUSTIS

PREPARED FOR
NATIONAL SCIENCE FOUNDATION
NSF G9705

TECHNICAL REPORT No. 1

DEPARTMENT OF MECHANICAL ENGINEERING
STANFORD UNIVERSITY
STANFORD, CALIFORNIA

JUNE 1, 1961

THE PLANE TURBULENT WALL JET
PART I - JET DEVELOPMENT AND FRICTION FACTOR

By

G. E. Myers, J. J. Schauer, and R. H. Eustis

Technical Report No. 1

Prepared Under National Science Foundation Grant
NSF G9705

Department of Mechanical Engineering
Stanford University
Stanford, California

June 1, 1961

ACKNOWLEDGEMENTS

The authors wish to acknowledge the assistance of the following people: Professors W. C. Reynolds and W. H. Schwarz made many helpful suggestions. Professor S. J. Kline provided the calibration facilities. P. W. Runstadler assisted with the hot-film measuring apparatus and the probe design. E. C. Steed constructed the hot-film probe. R. Krueger and B. G. Monteith took the data concerning the jet development.

The wall jet research program has been supported by the National Science Foundation.

ABSTRACT

The present paper is an investigation of the jet development, the velocity profiles, and the wall shearing stress in a two-dimensional, incompressible, turbulent wall jet. Experimental data concerning velocity profiles, decay of the maximum velocity and the jet growth are presented over greater ranges than previously available. The shearing stress, maximum velocity decay and jet thickness are predicted analytically by momentum-integral methods and the shear stress is measured experimentally by a hot-film technique. The hot-film values are checked by the wall shear stress computed from the measured velocity profiles.

Velocity profiles, velocity decay, and jet thickness agree well with previous investigators and the wall shear stress measurements help to resolve a wide divergence between the experimental values of the other investigators.

TABLE OF CONTENTS

LIST OF FIGURES

LIST OF TABLES

NOMENCLATURE

Arabic Symbols

A	constant defined by (20)
b	dimension of hot-film transverse to flow direction; in.
B	constant defined by (20)
c	specific heat; Btu/lbm°F
C	constant defined by (20)
C_f	friction factor, $2g_c\tau_w/\rho U^2$
D	constant defined by (20)
g_c	proportionality factor in Newton's Second Law; ft-lbm/lbf-sec^2
k	thermal conductivity; Btu/hrft°F
K	constant defined by (9)
ℓ	hot-film width; in.
L	jet nozzle thickness; in.
M	constant defined by (6)
P	dimensionless velocity profile in the inner layer, u/u_m
q	total heat transfer rate; Btu/hr
q"	heat transfer rate per unit area; Btu/hrft^2
Q	dimensionless velocity profile in the outer layer, u/u_m
r	non-dimensional variable defined by (16)
Re	slot Reynolds number, UL/ν
s	non-dimensional variable defined by (16)
t	non-dimensional variable defined by (16)
T	temperature; °F

u : velocity component in the x-direction; ft/sec

u^+ non-dimensional velocity, $u/\sqrt{g_c \tau_w/\rho}$

U velocity in the uniform core, initial jet velocity; ft/sec

v velocity component in the y-direction; ft/sec

x coordinate along wall in the jet direction; in.

$\tilde{x}$ coordinate along wall (see appendix); in.

y coordinate normal to wall; in.

y^+ non-dimensional distance, $(y/\nu)\sqrt{g_c \tau_w/\rho}$

Greek Symbols

α thermal diffusivity, $k/\rho c$; ft^2/hr

β defined by (39); in^{-2}

δ boundary layer thickness; in.

ζ non-dimensional coordinate normal to wall in jet layer, $(y - \delta_m)/(\delta - \delta_m)$

η non-dimensional coordinate normal to wall in inner layer, y/δ_m

κ constant in Prandtl's mixing hypothesis; ft/in

ν kinematic viscosity; ft^2/sec

ξ non-dimensional coordinate along wall, defined by (16)

ρ mass density; lbm/ft^3

σ defined in appendix as $9x/y^3$

τ shearing stress; lbf/ft^2

Subscripts

m	denotes condition at the maximum velocity point
o	denotes condition at the value of x where maximum velocity begins to decay
w	denotes condition at the wall
1	denotes condition at outer edge of uniform core
2	denotes condition in outer layer where $u = u_m/2$
∞	denotes condition outside thermal boundary layer

INTRODUCTION

As part of a research program studying the heat transfer and fluid mechanics of two-dimensional air jets impinging on flat plates, the present paper reports the fluid mechanics of the wall jet. The wall jet, in which the fluid flow is tangential to the solid surface, represents the limiting case of the impinging jet. By first attacking this simplified problem it is hoped that insight can be obtained which will be useful in the more complex impinging cases.

Although heat transfer between the solid wall and the fluid jet is the primary concern of the authors, it was felt that the friction factor should be measured since the experimental work previous to this paper has not been conclusive. Schwarz and Cosart[1] have made some shear measurements in which they obtained results about twice those found by Sigalla[2]. It was felt that some clarification was needed before continuing with the heat transfer work. This data would also provide a check on the analytical prediction of wall shear stress which must precede the heat transfer analysis.

The only analytical work which resulted in a useful prediction of the wall shear stress is that of Schwarz and Cosart. Glauert's[3] work with the turbulent wall jet, which is the only other analytical work on the subject found by the authors, does not include an analysis for the shearing stress in terms of convenient quantities.

Sigalla[2,4] has written two papers which include experimental shear data obtained by the method of Preston[5]. The wall shear results presented here, obtained by a hot-film technique, cover a more extensive range of variables and do not assume the flat plate "law of the wall" to hold for y^+ greater than 30. Data is taken out to 180 slot widths (Sigalla's went to 65) and the slot Reynolds number range is 7100 to 56,500 (Sigalla's was 22,800 to 52,200).

Schwarz and Cosart obtained their wall shearing stress

information by applying momentum-integral techniques to their measured velocity profiles. Förthmann[6] also used the momentum-integral method to obtain the shear distribution normal to the flat surface but does not show a variation along the plate.

As part of an investigation of a wall jet with an external stream, Bradshaw and Gee[7] have obtained some shear stress results for the ordinary wall jet. They find friction factors that are about six per cent higher than Sigalla's.

Although the work of Schwarz and Cosart, Bradshaw and Gee, and Förthmann are in agreement concerning velocity profile shape, decay of the maximum velocity and growth of the jet, similar information is presented in this report to establish confidence in the wall jet experimental apparatus and instrumentation.

The primary purpose of this work is to supply an analysis for the wall shearing stress and also to check and extend the previous experimental work on the wall jet. This report will also provide the basis for an analytical and experimental investigation of the heat transfer to wall jets.

ANALYTICAL DEVELOPMENT

Integral methods will be applied to the incompressible boundary layer equations to obtain a prediction for the wall shearing stress. The analysis will also give relations describing the decay of the maximum velocity and the boundary layer growth with distance.

The problem will be solved in two parts, (a) the "starting length" problem close to the nozzle exit where the maximum jet velocity has not yet begun to decay and (b) the region farther from the nozzle where the maximum velocity is decreasing. The solution for the first part will be used as the initial condition for the second part.

In solving each of these parts the flow will be divided into two regions. The region next to the wall, termed the "inner layer", will be assumed to behave very similarly to an ordinary turbulent boundary layer. The region away from the wall, or "outer layer", will be assumed to behave like a free jet. These two regions will be patched together at the point of maximum velocity.

It should be pointed out that complete similarity of the velocity profiles across the entire wall jet will not be assumed. Instead each layer will be taken to be similar within itself. This has the added generality that information concerning the mixing in the free jet layer can be incorporated in the analysis.

Figure 1 describes these various areas and helps to define the nomenclature to be used.

In each of these regions the momentum boundary layer equation will be used,

$$\frac{g_c \tau_y}{\rho} = uu_x + vu_y \qquad (1)$$

as well as the continuity equation,

$$u_x + v_y = 0 \qquad (2)$$

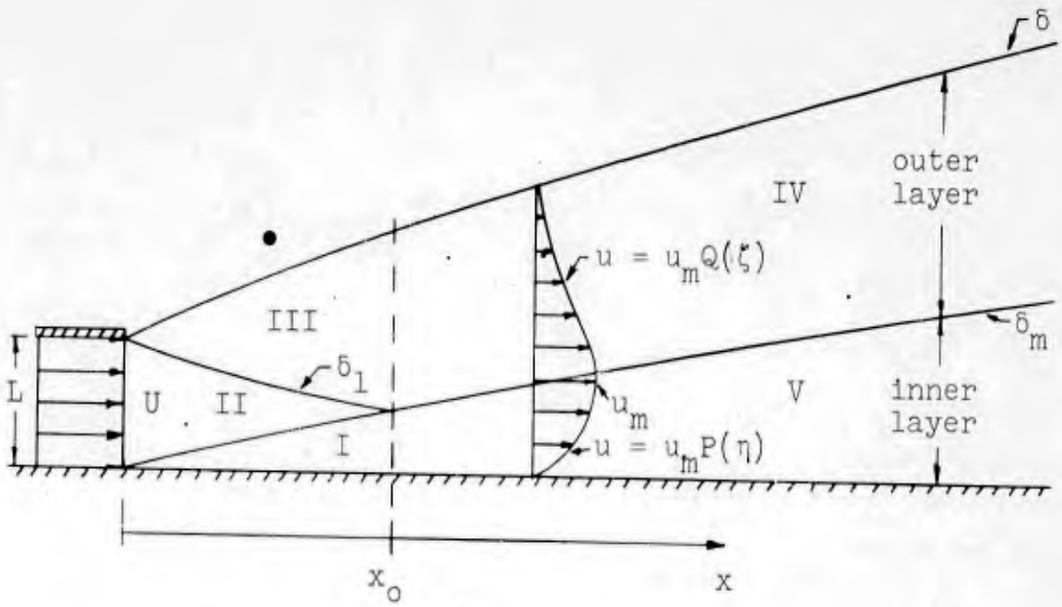

I, V: Inner or wall layer -- assumed to behave like a flat plate boundary layer

II: Uniform core -- region where $u = U$ which ends at $x = x_o$

III, IV: Free jet region or outer layer -- assumed to behave like free jet mixing

FIGURE 1. WALL JET NOMENCLATURE

In the wall layer the Blasius[+] relation,

$$\frac{g_c \tau_w}{\rho} = 0.0225 u_m^2 \left(\frac{u_m \delta_m}{\nu}\right)^{-1/4} \tag{3}$$

will be used to relate τ_w to u_m and δ_m. In the free jet layer the shearing stress will be assumed to be described by Prandtl's[++] hypothesis,

$$\frac{g_c \tau}{\rho} = \kappa u_m (\delta - \delta_m) u_y \tag{4}$$

where κ is an empirical constant.

The first step is solving the starting length problem to obtain information concerning conditions at x_o. First, we integrate (1) across the inner layer ($y=0$ to $y=\delta_m$) with the boundary conditions that $\tau(\delta_m) = 0$, $u=v=0$ at $y=0$ and $u=u_m=U$ at $y = \delta_m$. When this integrated equation is combined with (3) the following expression is found for δ_m:

$$\delta_m = M \frac{\nu^{1/5}}{U^{1/5}} x^{4/5} \tag{5}$$

where

$$M = \left[\frac{5(0.0225)}{4 \int_0^1 P(\eta)[1 - P(\eta)]d\eta}\right]^{4/5} \tag{6}$$

P and η being defined in the nomenclature section.

In region III, Eq. (4) is assumed to describe the mixing mechanism. This actually replaces (3) which was used for the inner layer. In addition to integrating (1) across the jet layer from δ_1 to δ, it is necessary to find some way that will allow inclusion of mixing information in the solution. Multiplying (1) by u before integrating gives a

---

[+]See Schlichting[8], page 432.

[++]See Schlichting, page 484.

second equation in which the information contained in (4) can be used. There are now two equations for the two unknowns δ_1 and δ. The boundary conditions are that $\tau(\delta_1) = \tau(\delta) = 0$, $u(\delta_1) = U$ and $u(\delta) = 0$.

These equations yield

$$\frac{\delta_1}{L} = 1 + \left[1 - \int_0^1 P(\eta)d\eta\right] \frac{\delta_m}{L} - K \frac{x}{L} \tag{7}$$

and

$$\frac{\delta - \delta_1}{L} = \frac{K}{\int_0^1 Q^2(\zeta)d\zeta} \frac{x}{L} \tag{8}$$

where Q and ζ are defined under nomenclature and

$$K = \frac{2\kappa \int_0^1 Q'^2(\zeta)d\zeta \int_0^1 Q^2(\zeta)d\zeta}{\int_0^1 Q^2(\zeta)d\zeta - \int_0^1 Q^3(\zeta)d\zeta} \tag{9}$$

The conditions at x_o are then found to be

$$\frac{\delta_{m_o}}{L} = \frac{M}{Re^{1/5}} \left(\frac{x_o}{L}\right)^{4/5} \tag{10}$$

and

$$\frac{\delta_o - \delta_{m_o}}{L} = \frac{K}{\int_0^1 Q^2(\zeta)d\zeta} \frac{x_o}{L} \tag{11}$$

The value of x_o/L is determined from (7) and(10) by setting $\delta_1 = \delta_m$ when $x = x_o$. Thus, x_o must satisfy

$$\frac{M \int_0^1 P(\eta)d\eta}{Re^{1/5}} \left(\frac{x_o}{L}\right)^{4/5} = 1 - K \frac{x_o}{L} \tag{12}$$

If representative values for K, M, Re and $\int_0^1 P(\eta)d\eta$ are chosen, it can be shown that by changing Re

by a factor of ten the effect upon x_o is less than ten per cent. Therefore x_o will be taken to be independent of Re to simplify the analysis.

Having solved the starting length problem, the next step is to apply the same equations to regions IV and V using (10) and (11) as initial conditions. In this portion of the flow the maximum velocity, u_m, is a variable in place of δ_1 which was used in the starting length problem. Again there are three unknowns (u_m, δ_m and δ) which means that three equations will be needed.

In the inner layer we integrate (1) from $y=0$ to $y=\delta_m$, using (2) and (3) as before. The boundary conditions are $\tau(\delta_m) = 0$, $u(\delta_m) = u_m$ and $u(0) = v(0) = 0$. This gives

$$0.0225 \frac{\nu^{1/4}}{u_m^{1/4}\delta_m^{1/4}} u_m^2 = u_m \frac{d}{dx}(\delta_m u_m) \int_0^1 P(\eta)d\eta - \frac{d}{dx}(u_m^2\delta_m) \int_0^1 P^2(\eta)d\eta \qquad (13)$$

In the outer layer we integrate (1) from $y = \delta_m$ to $y = \delta$ using (2) and the boundary conditions $\tau(\delta_m) = \tau(\delta) = 0$, $u(\delta_m) = u_m$ and $u(\delta) = 0$. This results in the following relation

$$\int_0^1 Q^2(\zeta)d\zeta \frac{d}{dx}[u_m^2(\delta - \delta_m)] + u_m \frac{d}{dx}(u_m\delta_m) \int_0^1 P(\eta)d\eta = 0 \qquad (14)$$

As in the starting length problem it was found necessary to obtain the third equation by multiplying (1) through by u before integrating and using (4) to give

$$\int_0^1 Q^3(\zeta)d\zeta \frac{d}{dx}[u_m^3(\delta - \delta_m)] + \int_0^1 P(\eta)d\eta u_m^2 \frac{d}{dx}(\delta_m u_m) + 2\kappa u_m^3 \int_0^1 Q'^2(\zeta)d\zeta = 0 \qquad (15)$$

Equations (13), (14) and (15) are the three equations which must be solved simultaneously. It was found convenient to introduce the following non-dimensional variables:

$$r = \frac{\delta_m u_m}{\delta_{m_o} U}$$

$$s = \frac{(\delta - \delta_m)u_m^2}{(\delta_o - \delta_{m_o})U^2} \qquad (16)$$

$$t = \frac{u_m}{U}$$

$$\xi = \frac{x}{x_o}$$

By so doing we arrive at the following set of equations:

$$At^2 \frac{dr}{d\xi} + t \frac{ds}{d\xi} + s \frac{dt}{d\xi} = -Dt^3 \qquad (17)$$

$$Bt \frac{dr}{d\xi} + \frac{ds}{d\xi} = 0 \qquad (18)$$

$$Ct \frac{dr}{d\xi} - r \frac{dt}{d\xi} = \frac{4C}{5} t^2 r^{-1/4} \qquad (19)$$

with the initial conditions that $r(1) = s(1) = t(1) = 1$. A, B, C and D are constants depending upon the assumed choice of velocity profiles [$P(\eta)$ and $Q(\zeta)$] and upon δ_{m_o} and δ_o which are determined from the starting length problem. It can be shown that

$$A = \frac{\delta_{m_o}}{(\delta_o - \delta_{m_o})} \frac{\int_0^1 P(\eta)d\eta}{\int_0^1 Q^3(\zeta)d\zeta} \qquad C = \frac{\int_0^1 P(\eta)d\eta - \int_0^1 P^2(\eta)d\eta}{\int_0^1 P^2(\eta)d\eta} \qquad (20)$$

$$B = \frac{\delta_{m_o}}{(\delta_o - \delta_{m_o})} \frac{\int_0^1 P(\eta)d\eta}{\int_0^1 Q^2(\zeta)d\zeta} \qquad D = \frac{\int_0^1 Q^2(\zeta)d\zeta - \int_0^1 Q^3(\zeta)d\zeta}{\int_0^1 Q^3(\zeta)d\zeta}$$

Although (17) to (19) show no explicit Reynolds number parameter, this effect is found implicitly in the constants A and B which contain δ_{m_o} and δ_o. The value of δ_{m_o} and δ_o are determined by solving (10), (11) and (12). Taking $\kappa = 0.014$ ft/12 in which is given by Schlichting[+] for free jets and assuming

$$P(\eta) = \eta^{1/7} \quad , \quad Q(\zeta) = (1 - \zeta^2)^2 \quad , \quad Re = 45{,}000$$

an example solution of Eqs. (17) to (19) was obtained numerically.

It was observed that the solution so obtained was within 2 per cent of the one found by taking $\kappa = \infty$ or $\delta_{m_o} = 0$. The conclusion is that the behavior of u_m, δ_m and δ depend largely upon the free jet characteristics. By approximating $\delta_{m_o} = 0$, or $A = B = 0$, an analytical solution can be obtained, thus avoiding a numerical solution. This approximation becomes better at higher Reynolds numbers. It does have the disadvantage that some information is lost which might be gained from a more detailed solution but this is not considered a drawback since the numerical solution is so close to the approximate one.

The solution to Eqs. (17), (18), and (19) under this simplifying assumption is

$$t = \frac{1}{\sqrt{1 + 2D(\xi - 1)}} \tag{21}$$

$$r = \left\{ \left[1 - \frac{1}{D(1 + 5/4C)} \right] t^{5/4C} + \frac{1}{D(1 + 5/4C)} t^{-1} \right\}^{4/5} \tag{22}$$

$$s = 1 \tag{23}$$

To obtain the shear stress prediction, Eqs. (10) and (16) are used in (3) to replace u_m and δ_m by r and t.

[+]See Schlichting[8], page 492.

After defining a friction factor we obtain

$$C_f Re^{1/5} = \frac{0.045}{M^{1/4}} \frac{t^2 r^{-1/4}}{(x_o/L)^{1/5}} \qquad (24)$$

When (21), (22) and (23) are unraveled the following expressions are found for u_m and δ_2 :

$$\frac{u_m}{U} = t = \frac{1}{\sqrt{1 + 2D\left[\left(\frac{x}{L}\Big/\frac{x_o}{L}\right) - 1\right]}} \qquad (25)$$

$$\frac{\delta_2}{L} = \frac{\zeta_2}{\left[\frac{Re^{1/5}}{M\left(\frac{x_o}{L}\right)^{4/5} \int_0^1 P(\eta)d\eta}\right] t^2 \int_0^1 Q^2(\zeta)d\zeta} \left\{\left[\frac{Re^{1/5}}{M(x_o/L)^{4/5} \int_0^1 P(\eta)d\eta}\right] - 1 + \frac{rt \int_0^1 Q^2(\zeta)d\zeta}{\zeta_2 \int_0^1 P(\eta)d\eta}\right\} \qquad (26)$$

where r is still given by (22) and ζ_2 is given by $Q(\zeta_2) = 1/2$.

It is necessary to make an assumption concerning the shape of the velocity profile and also x_o/L in order to obtain a numerical result. Since we are assuming the inner layer to behave much like a flat plate it is reasonable to assume $P(\eta) = \eta^{1/7}$. Based on experience with free jet work, the outer layer profile is assumed to be $Q(\zeta) = (1 - \zeta^2)^2$. Experimental evidence is inconclusive concerning the value of x_o/L . Some preliminary results indicate that $4 \leq x_o/L \leq 14$. We have taken $x_o/L = 7$ since it is in the correct range and provides a reasonable fit to our data.

With these assumptions the analysis gives

$$\frac{u_m}{U} = t = \frac{1}{1 + 0.381\left(\frac{x/L}{7} - 1\right)} \tag{27}$$

$$r = \left[0.523\ t^{10} + 0.477\ t^{-1}\right]^{4/5} \tag{28}$$

$$\frac{\delta_2}{L} = \frac{2.05}{t^2 Re^{1/5}}\left[0.650\ Re^{1/5} - 1 + 0.857\ rt\right] \tag{29}$$

$$C_f Re^{1/5} = 0.0391\ t^2 r^{-1/4} \tag{30}$$

These are the equations shown in Figs. 7, 8 and 9.

Asymptotic solutions can be found for large values of x where the similarity approximations become more valid. In this region Eqs. (21) to (23) give the solutions

$$t = \frac{1}{\sqrt{2D}} \frac{(x/L)^{-1/2}}{(x_o/L)^{-1/2}} \tag{31}$$

$$r = \frac{(2/D)^{2/5}}{(1 + 5/4C)^{4/5}} \frac{(x/L)^{2/5}}{(x_o/L)^{2/5}} \tag{32}$$

$$s = 1 \tag{33}$$

From these it can be shown that

$$u_m \sim x^{-1/2}$$

$$\delta_m \sim x^{9/10} \tag{34}$$

$$\delta - \delta_m \sim x^1$$

and

$$C_f Re^{1/5} = \frac{0.045}{M^{1/4}} \left(\frac{1}{2} + \frac{5}{8C} \right)^{1/5} \left(\frac{x_o}{2DL} \right)^{9/10} \left(\frac{x}{L} \right)^{-11/10} \qquad (35)$$

Since the analysis for δ_2 does not show a strong dependence upon Reynolds number (see Fig. 8), Eq. (26) can be simplified by letting $Re \to \infty$. This gives

$$\frac{\delta_2}{L} = \frac{\zeta_2}{\int_0^1 Q^2(\zeta) d\zeta} t^{-2} \qquad (36)$$

which means that for large x, $\delta_2 \sim x$.

EXPERIMENTAL APPARATUS AND PROCEDURE

The wall jet was formed by a converging nozzle with one side of its exit section flush with a hydraulically smooth plate 96 inches long, as shown in Fig. 2. The nozzle had a contraction ratio of 40:1 and a nozzle exit measuring 1/2 by 60 inches. Velocity profiles taken at the nozzle exit section showed the velocity to be uniform to within $\pm$ 1.5 per cent for ninety per cent of the 1/2 inch slot width over the entire 60 inches.

In order to maintain two-dimensionality in the flow, nine inch high sidewalls were installed along the outer edges of the plate. Since it was found that the velocity was within 10 per cent of its centerline value for a distance of 15 inches on either side of the centerline, the wall jet was considered to be sufficiently two-dimensional.

The velocity measurements near the wall utilized a flattened, total-head tube with an opening about 0.002 by 0.020 inches. Further from the wall a Kiel probe was employed to avoid the sensitivity to flow direction which the other probe exhibited. The results of the velocity surveys are discussed in the next section.

The shearing stress was measured by a hot-film technique. This method, proposed by Ludwieg[9] and developed further by Liepmann and Skinner[10], is based on the principle that the heat transfer from a small heated element flush with the surface of a wall is related to the shearing stress at that point. This relation is developed in the appendix.

A photograph and a drawing of the hot-film plug are shown in Fig. 3. The narrow platinum film is baked on a hollow glass stem. The stem is then isolated from the plate by a Kel-F retainer of very low thermal conductivity.

The film has energy losses by conduction through the stem and by radiation which are not included in the convection problem analyzed in the appendix. These and other

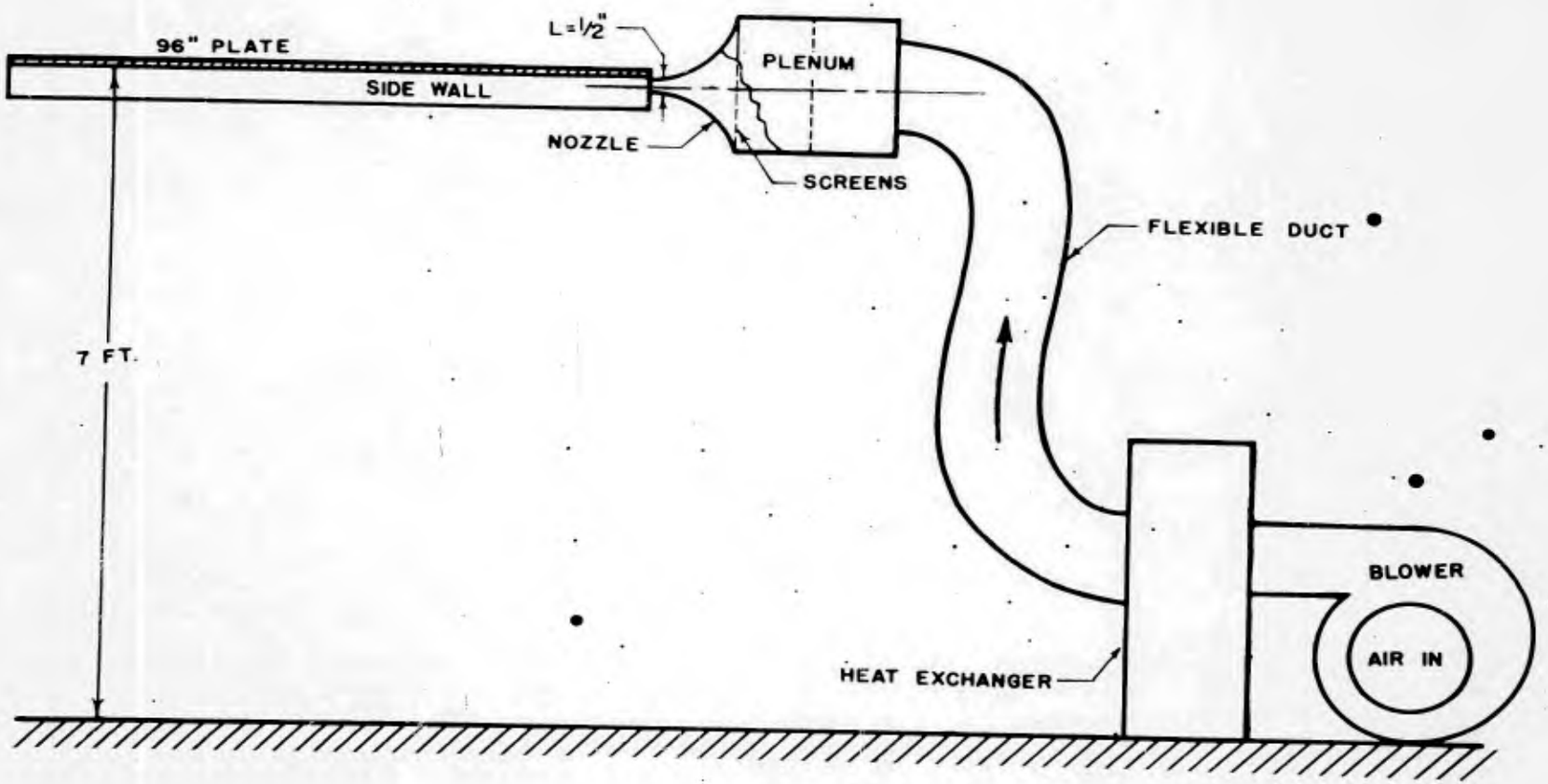

FIGURE 2. SCHEMATIC OF EXPERIMENTAL APPARATUS

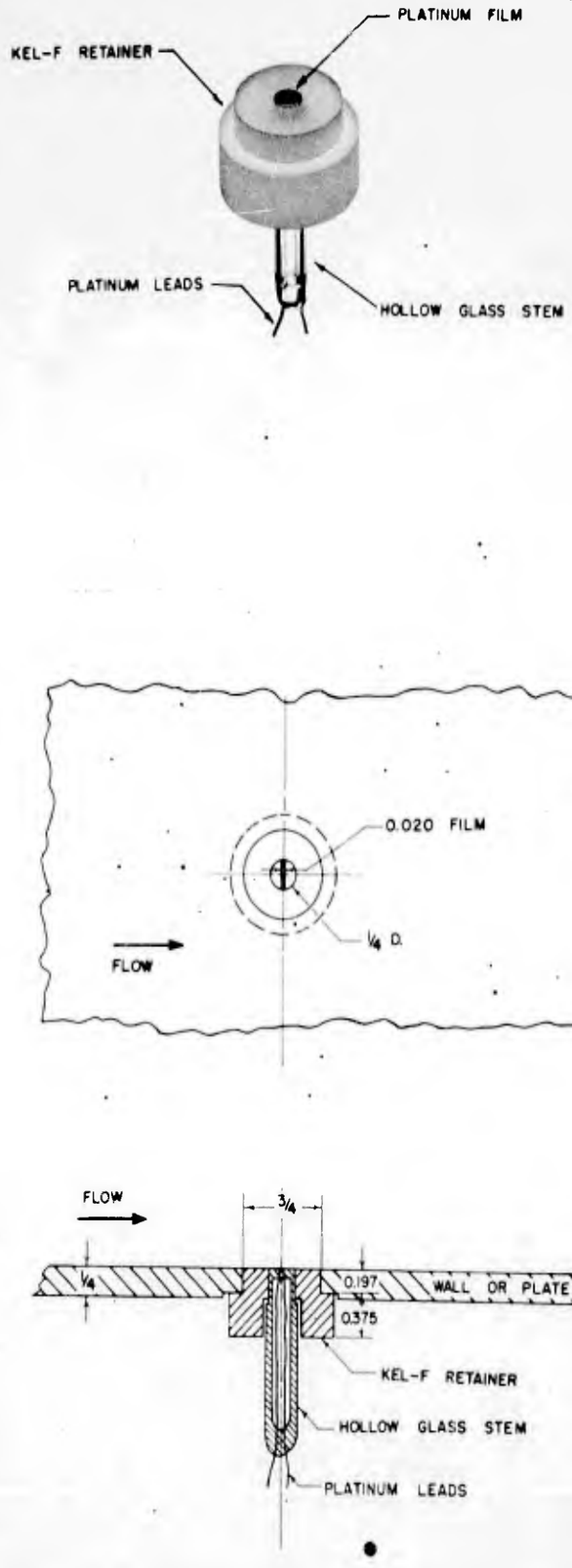

FIGURE 3. PHOTOGRAPH AND DETAILED DRAWING OF WALL SHEAR PLUG

deviations from the idealized model are included by calibrating the film and its immediate surroundings in a flow very similar to the flow in which the actual shear measurements are to be made. The calibration for the turbulent wall jet measurements was performed on a flat plate with a turbulent boundary layer and a zero pressure gradient designed by Lisin[11]. Velocity profiles taken on this plate were standard and the shear at the point of calibration was computed from an empirical fit[+] to numerous data taken on such plates.

The calibration curve was taken at constant film resistance. The shear was varied by changing the free stream velocity over the flat plate and a meter reading related to the voltage drop across the film was obtained at each wall shearing stress. The entire plug is calibrated in the flat plate configuration and then transferred to the wall jet. The plug was calibrated before and after each run of data as a precaution against drifting of the electronic equipment. A typical calibration curve, with data from several days, is shown in Fig. 4. The assumption which is made in using a standard flat plate to calibrate the hot-film for shear measurements to be made with the wall jet is that the velocity profiles are similar over the thickness of the thermal boundary layer. Since the maximum thickness of the thermal boundary layer was about $y^+ = 10$ (see appendix), this assumption is well substantiated as discussed later in regard to Fig. 11.

Shear data were taken on the plate centerline by inserting the calibrated hot-film assembly at prepared locations six inches apart. Runs were taken both by holding the jet velocity constant while varying the plug location and by holding the plug location constant while varying the jet velocity.

[+]See Schlichting[8], page 438.

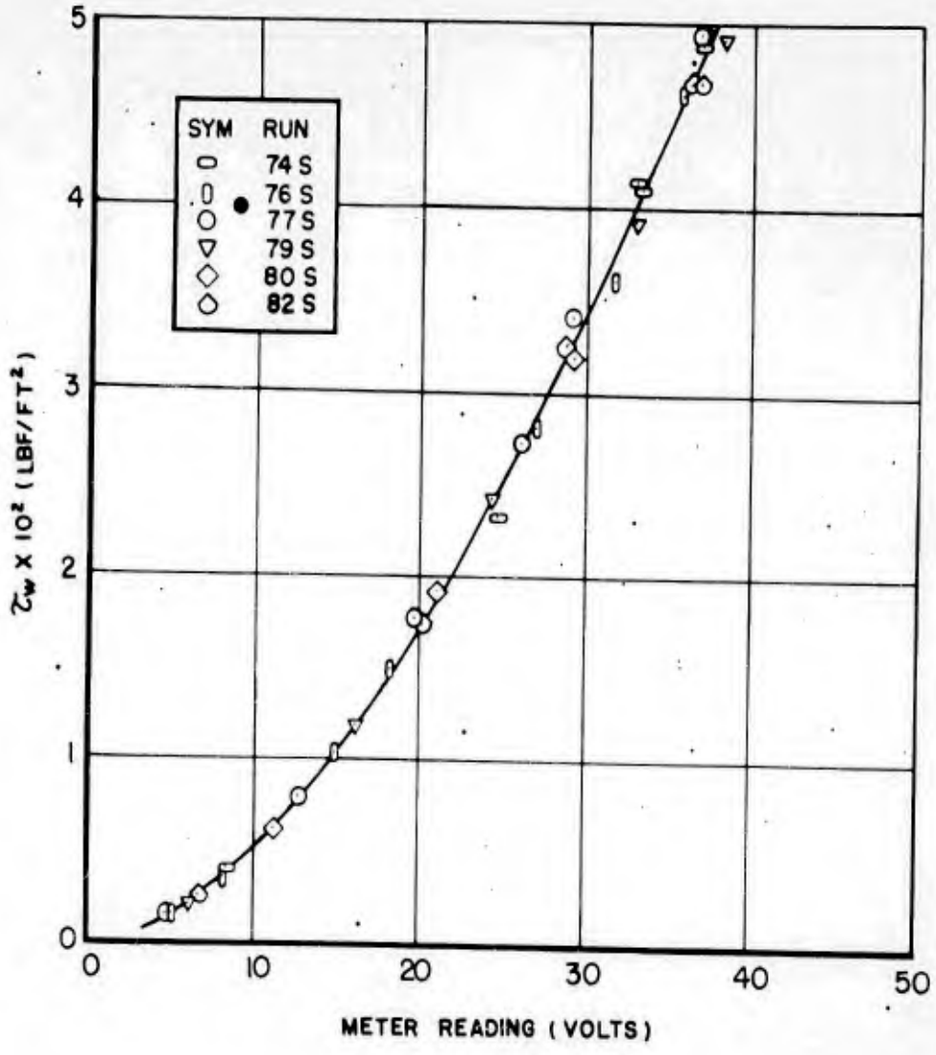

FIGURE 4. TYPICAL CALIBRATION OF WALL SHEAR PLUG

WALL JET DEVELOPMENT RESULTS

The experimental investigation of the wall jet development was undertaken to insure that the velocity profiles were consistent with those measured by Schwarz and Cosart[1], Sigalla[2], and Bradshaw and Gee[7]. Confidence would then be established in the present wall jet apparatus. This investigation was also expected to show similarity over an extended x/L range at different Reynolds numbers.

The velocity profiles, as shown in Fig. 5, were similar for the two Reynolds numbers and for x/L greater than 24 out to x/L of 180, the limit of the data. These profiles agreed with those published by other workers. A plot of the inner layer, as shown in Fig. 6, also agrees with a similar plot by Schwarz and Cosart and further supports their contention that, for regions away from the wall, the best fit to the data in the form $u/u_m = (y/\delta_m)^{1/n}$ is for n closer to 14 than to the more common value of 7.

The decay of the maximum velocity is an important factor in the wall jet development. The data seemed to show a slight Reynolds number effect with the higher Reynolds numbers exhibiting a slower velocity decay. The analysis, however, predicted no Reynolds number effect and a special test to measure u_m for several jet velocities and distances from the nozzle failed to show any clearly defined variation of the decay with Reynolds number. The decay of u_m versus x/L is shown in Fig. 7.

The wall jet growth, Fig. 8, was predicted quite well by the analysis. The effect of Reynolds number on this growth was predicted to be small by the analysis and no effect could be observed in the data. In common with other investigators, no correction was made in the velocity measurements for turbulence since these measurements were not made for the conditions reported. The turbulence level in the outer layer at $y = \delta_2$ is rather high as indicated by

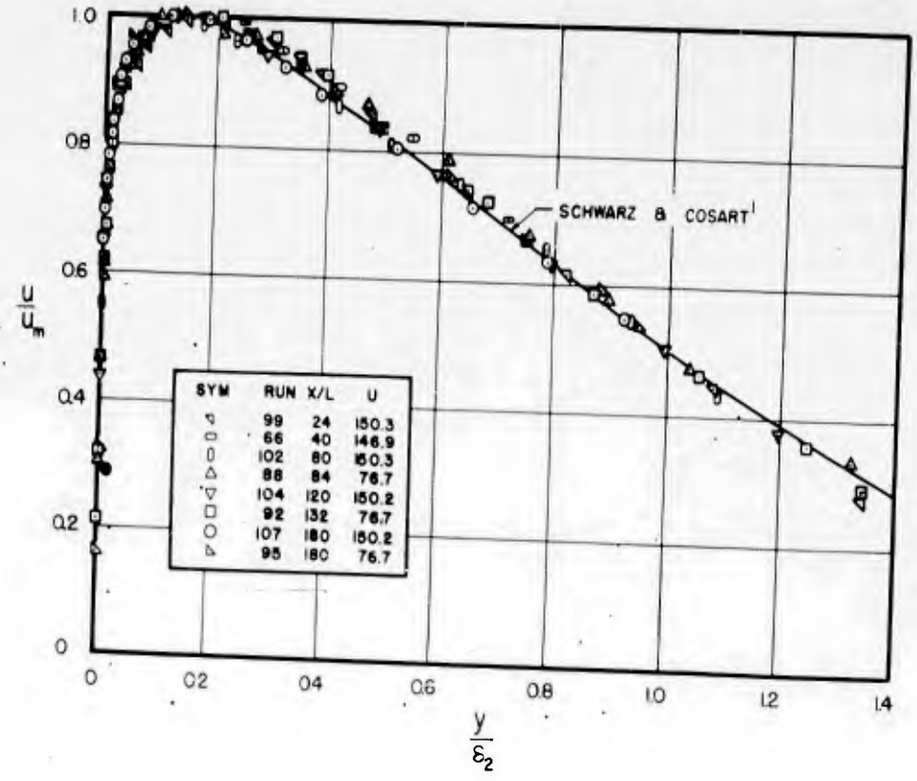

FIGURE 5. WALL JET VELOCITY PROFILES

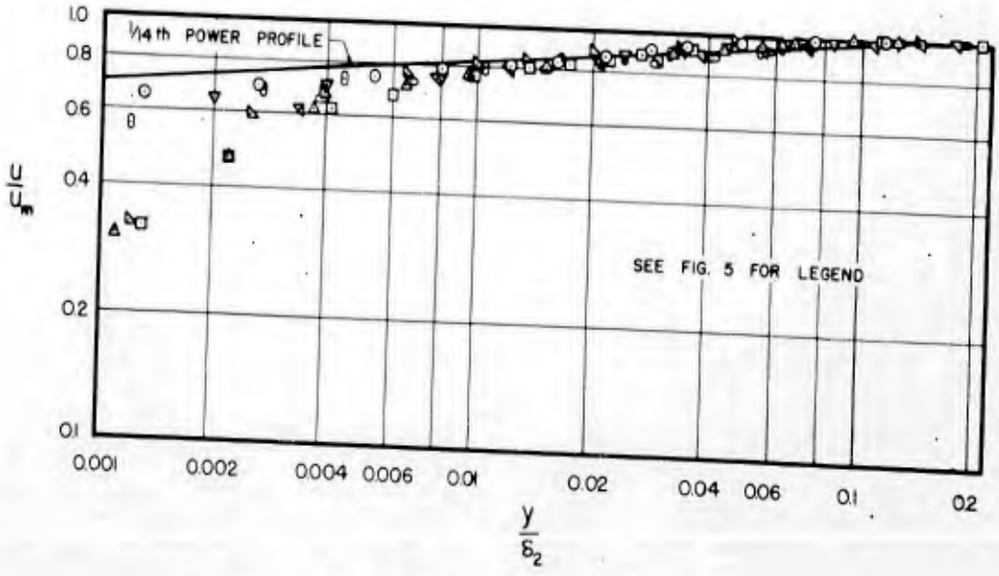

FIGURE 6. WALL JET INNER LAYER VELOCITY PROFILES

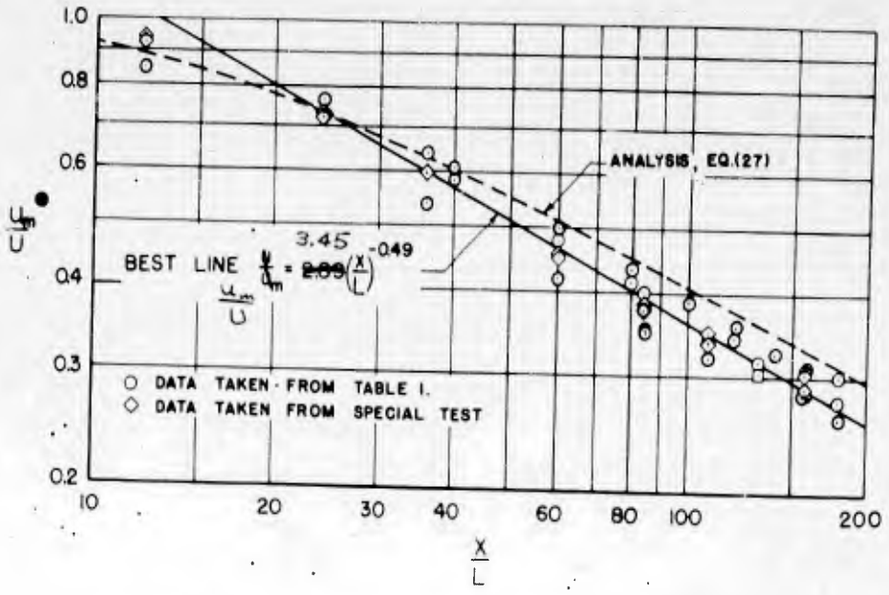

FIGURE 7. WALL JET MAXIMUM VELOCITY DECAY

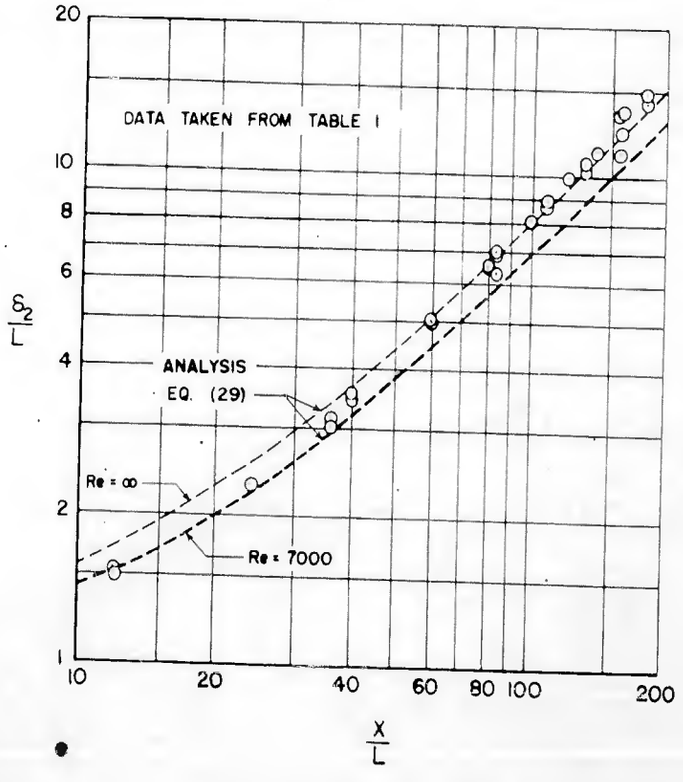

FIGURE 8. WALL JET GROWTH

the 40 per cent value given by Bradshaw and Gee, and the correction is on the order of eight per cent of the velocity. The effect of this correction would be to lower δ_2/L .

It was concluded from the agreement of the velocity profiles, the maximum velocity decay and the jet growth with the measurements of other workers that the wall jet investigated in this report was representative of two-dimensional wall jets.

WALL JET FRICTION FACTOR RESULTS

Wall jet friction factor information, obtained with the hot-film, is presented in Fig. 9 which covers a more extensive range of x/L and Re than has been previously reported. The data extends out to 180 slot widths and the Reynolds number varied between 7100 and 56,500. It should be noted that the friction factor used throughout this report differs from that defined by previous workers in that the normalizing velocity is U and not u_m. It is felt that this has more engineering usefulness since a second plot is not now required to first find u_m before evaluating τ_w.

An attempt was made to correlate the shearing stress data in the form $C_f Re^n$ as a function of $(x/L)Re^m$ in order to include the Reynolds number effects. The best correlation is shown in Fig. 9 where $n = 1/4$ and $m = -1/6$. These compare with values from the analysis of $n = 1/5$ and $m = 0$. The difference between the best fit and the analysis is on the order of $Re^{7/60}$. This was thought, in part, to be due to the assumption that κ_o was not a function of Re.

A least-squares line was fit to the data for $(x/L)Re^{-1/6}$ greater than 4.5. This line was found to be given by

$$C_f Re^{1/12}(x/L) = 0.1976 \qquad (37)$$

Although the interval in which a future single data point would be expected to fall, at 20 to 1 odds, is $\pm$ 18 per cent, the average of future data points can be expected to be within $\pm$ 4 per cent of the line given by Eq. (37) for $4.5 < (x/L)Re^{-1/6} < 37.0$.

As a check on the hot-film measurements a method described by Clauser[12] was used to obtain the wall shearing stress from the measured velocity profiles. In order to apply this method it was necessary to assume the validity of

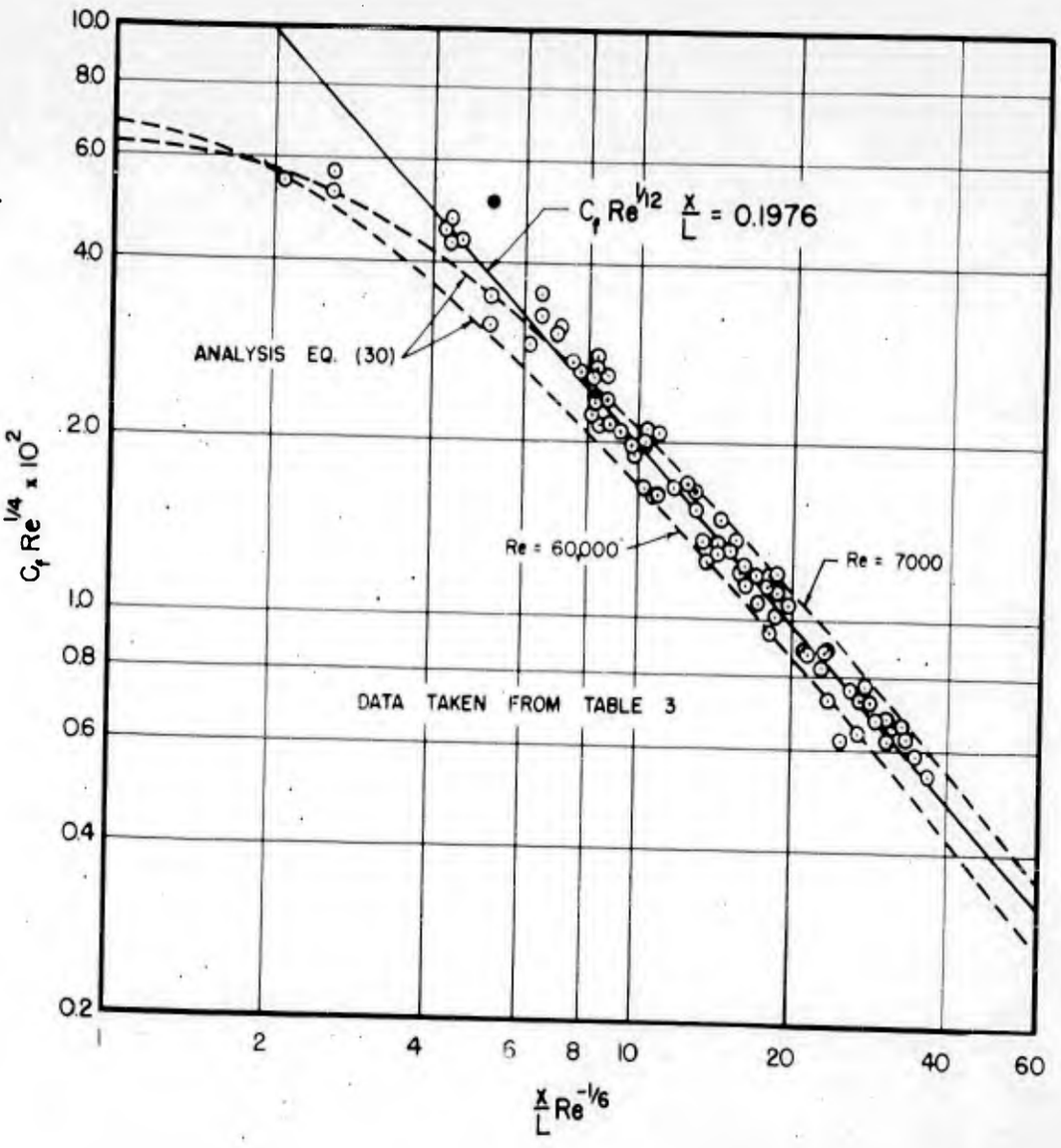

FIGURE 9. WALL JET FRICTION FACTOR

the "law of the wall" in the region $10 < y^+ < 30$ for the wall jet. The values found in this manner agree very well with the hot-film data as shown in Fig. 10.

It is also of interest in boundary layer studies to correlate velocity profile data in the dimensionless form u^+ vs. y^+. These results are shown in Fig. 11 for the same profiles given in Figs. 5 and 6. Viscous[13,14] and velocity gradient[15] corrections were applied to the total head tube readings as in Fig. 6. Equation (37) was used to calculate the value of τ_w needed in the normalization. It is seen that the flat plate "law of the wall" correlation holds also for the wall jet for y^+ up to about 30. The scatter in the data at low values of y^+ is due to the larger relative uncertainty in probe location as the probe approaches within a few thousandths of an inch to the wall.

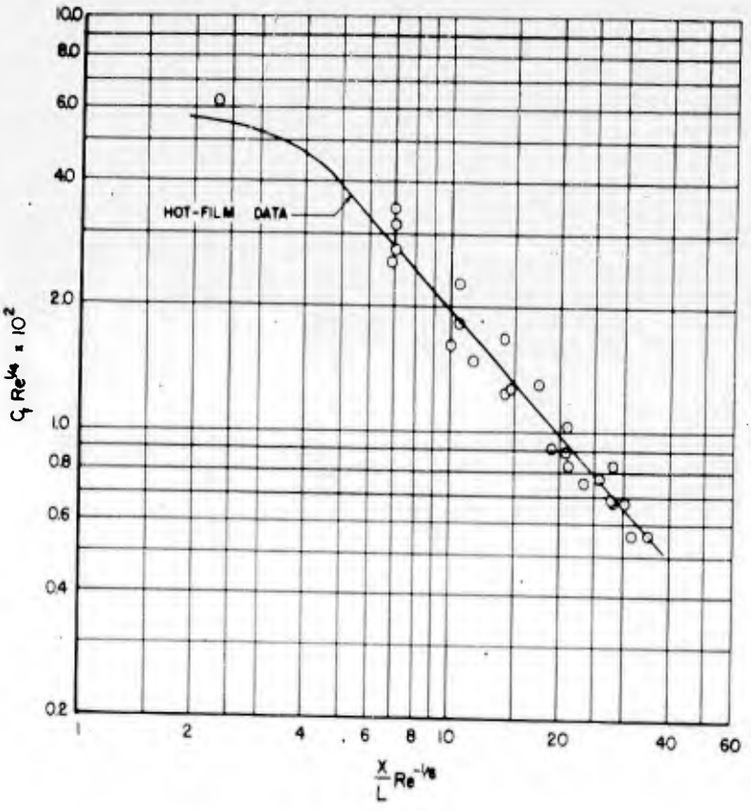

FIGURE 10. COMPARISON OF FRICTION FACTOR VALUES OBTAINED FROM HOT-FILM METHOD WITH THOSE FROM VELOCITY PROFILES

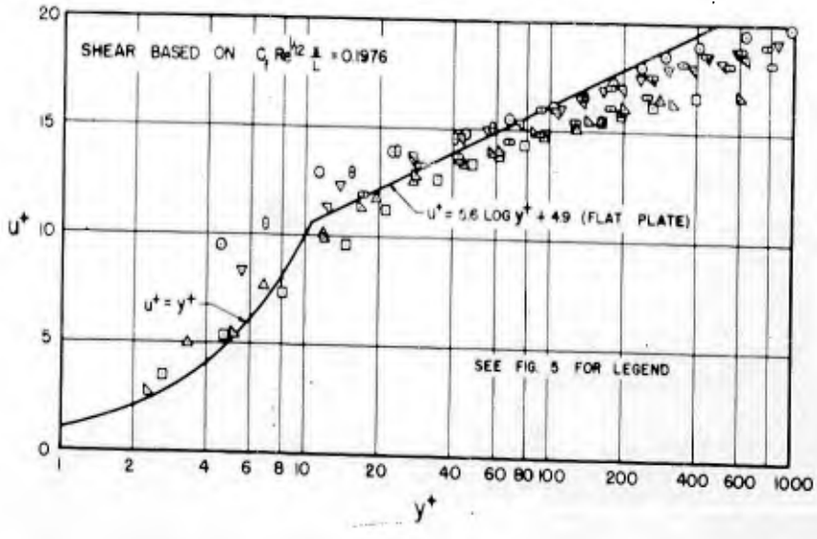

FIGURE 11. COMPARISON BETWEEN WALL JET AND FLAT PLATE VELOCITY PROFILES

DISCUSSION

Data have been presented for the incompressible, turbulent wall jet to show (i) velocity profiles, (ii) maximum velocity decay with distance, (iii) boundary layer growth with distance, and (iv) wall shear stress variation with distance.

The velocity profiles obtained are similar to those of earlier investigators and confirm Schwarz and Cosart's[1] statement that the wall jet inner layer velocity profile is closer to $u/u_m = (y/\delta)^{1/14}$ than $(y/\delta)^{1/7}$. The velocity profile data also show that the flat plate "law of the wall" holds for the wall jet for y^+ up to 30 but does not represent the wall jet over the extended y^+ range (up to 1000) usually assumed valid for flat plates in an infinite stream.

Schwarz and Cosart reported the maximum velocity to vary as $x^{-0.555 \pm 0.05}$ whereas the present work shows the variation to be $x^{-0.49 \pm 0.03}$. The data also show no effect of Reynolds number upon the velocity decay.

The boundary layer thickness is shown to grow as $x^{0.95 \pm 0.03}$ for x/L greater than 25. Again, no Reynolds number effect could be detected.

A comparison of the present shear data with that of Schwarz and Cosart and Sigalla[2], see Fig. 12, shows the shear to be 15 per cent higher than Sigalla's but 50 per cent lower than Schwarz and Cosart. It is felt that Sigalla's Preston tube technique may have produced low shear readings since the tube extended as far as $y^+ = 150$. This is because Sigalla's calibration is dependent upon the flat plate "law of the wall" holding for the wall jet in this region. With a smaller Preston tube, Bradshaw and Gee[7] measured friction factors about six per cent higher than Sigalla.

The high shear values reported by Schwarz and Cosart may be due to the sensitivity of their results to the determination of the x-derivative of $u_m^2\delta_2$. A 2 per cent

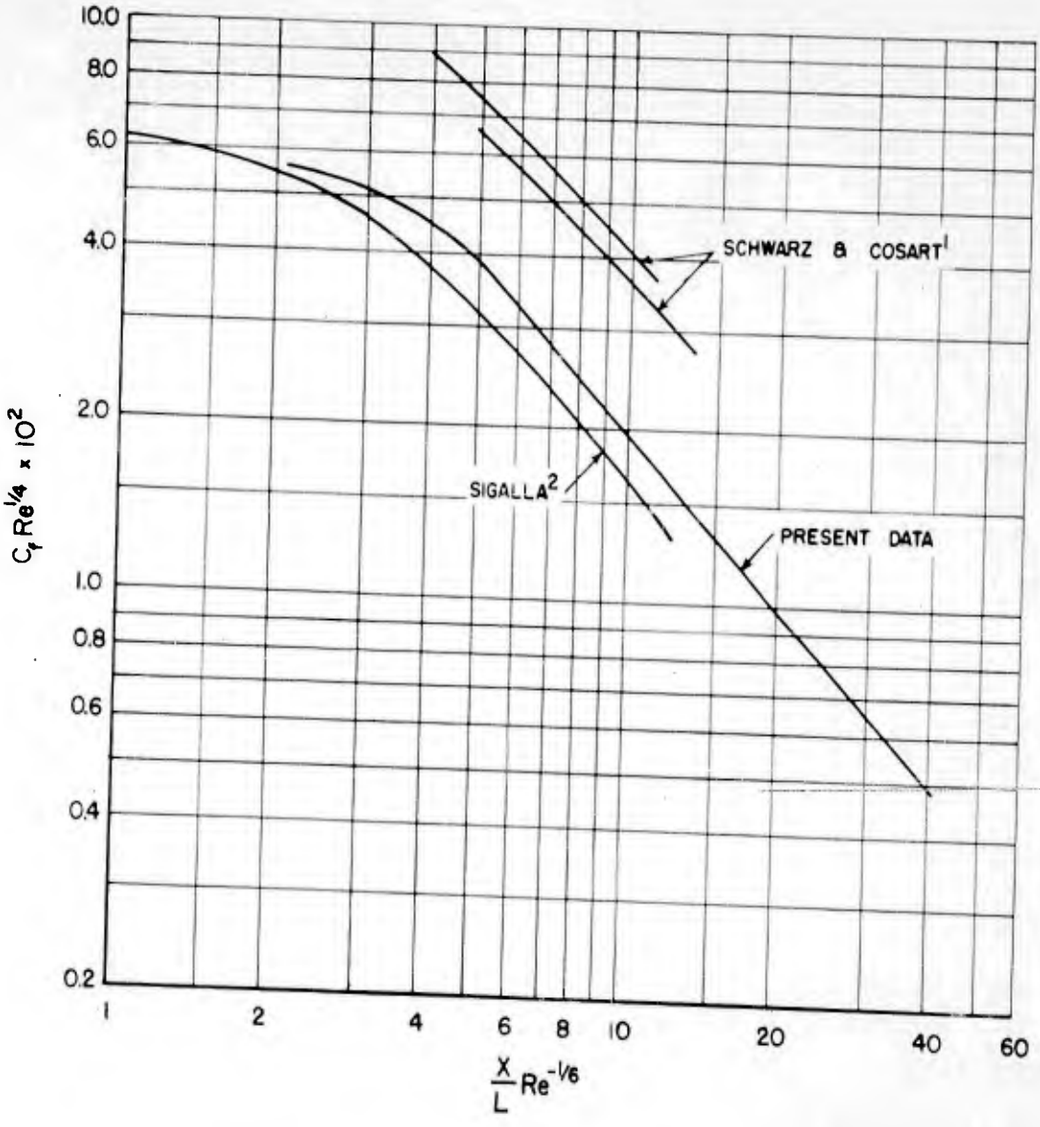

FIGURE 12. COMPARISON OF EXISTING WALL JET FRICTION FACTOR DATA

error in the value of the exponent they found for the velocity decay would introduce a 20 per cent error in the friction factor reported.

The analytical results are in agreement with the work of other investigators as shown below:

	u_m	δ
Plane free jet (Schlichting)	$x^{-0.5}$	x
Plane boundary layer (Schlichting)	x^{0}	$x^{0.8}$
Plane wall jet (Schwarz and Cosart)	$x^{-0.555}$	x
Plane wall jet (Glauert)	$x^{-0.583}$	x
Plane wall jet (present analysis, large x)	$x^{-0.5}$	x

The solutions for u_m, Eq. (25), and δ_2, Eq. (26), are more complicated than the simple power relations found by other investigators. This arises from the fact that complete similarity between the inner and outer layers of the wall jet was not assumed.

It is seen that the variation of u_m in the present analysis is the same as for the plane free jet. This is a reasonable result in view of the fact that the assumption of infinite eddy viscosity in the outer layer, or $A = B = 0$, let to a good approximation to the more exact numerical solution. Physically, this says that the free jet portion, or outer layer, of the flow plays a determining role in the wall jet. Bradshaw and Gee have also noted this fact.

REFERENCES

1. W. H. Schwarz and W. P. Cosart, "The Two-Dimensional Turbulent Wall-Jet", Jour. of Fluid Mech., to be published.

2. A. Sigalla, "Measurements of Skin Friction in a Plane Turbulent Wall Jet", Jour. Royal Aero. Soc., Vol. 62, No. 576, Dec. 1958, pp. 873-877.

3. M. B. Glauert, "The Wall Jet", Jour. of Fluid Mech., Vol. 1, Dec. 1956, pp. 625-643.

4. A. Sigalla, "Experimental Data on Turbulent Wall Jets", Aircraft Engineering, Vol. 30, May 1958, pp. 131-133.

5. J. H. Preston, "The Determination of Turbulent Skin Friction by Means of Pitot Tubes", Jour. Royal Aero. Soc., Vol. 58, Feb. 1954, p. 109.

6. E. Förthmann, "Turbulent Jet Expansion", NACA TM 789, 1934.

7. P. Bradshaw and M. T. Gee, "Turbulent Wall Jets With and Without an External Stream", A.R.C. 22,C08, F.M. 2971, 1960.

8. H. Schlichting, "Boundary Layer Theory", McGraw-Hill Book Company, Inc., New York, N. Y., 1955.

9. H. Ludwieg, "Instrument for Measuring the Wall Shearing Stress of Turbulent Boundary Layers", NACA TM 1284, 1950.

10. H. W. Liepmann and G. T. Skinner, "Shearing-Stress Measurements by Use of a Heated Element", NACA TN 3268, 1954.

11. S. J. Kline, A. V. Lisin and B. A. Waitman, "An Experimental Investigation of the Effect of Free Stream Turbulence on the Turbulent Boundary Layer Growth", Rep. MD-2, NACA Contract NAw-6500, Dept. of Mech. Engrg., Stanford, Calif. 1958.

12. F. H. Clauser, "Turbulent Boundary Layers in Adverse Pressure Gradients", Jour. of Aero. Sci., Feb.1954,p. 91.

13. W. R. Schowalter and G. E. Blaker, "On the Behavior of Impact Tubes at Low Reynolds Numbers", Trans. ASME, Vol. 83, Series E, March 1961.

14. C. W. Hurd, K. P. Chesky, and A. H. Shapiro, "Influence of Viscous Effects on Impact Tubes", Jour. of Applied Mechanics, 1953, p. 253.

15. R. C. Dean, "Aerodynamic Measurements", Gas Turbine Laboratory, M.I.T., 1953.

TABLE 1. WALL JET DEVELOPMENT

RUN	U ft/sec	Re x 10^{-3}	x/L	δ_p/L	u_m/U
66	146.9	35.8	40	3.56	0.593
67	152.0	36.5	36	3.19	0.640
68	152.0	36.5	60	5.09	0.477
69	147.0	35.7	80	6.54	0.412
71	152.0	36.5	84	6.80	0.400
73	152.2	36.4	108	8.64	0.339
74	147.0	35.7	120	9.88	0.341
76	152.2	36.4	132	10.19	0.318
78	146.9	35.4	150	11.14	0.308
79	149.4	35.8	158	12.26	0.284
81	150.0	35.5	180	13.97	0.277
83	79.8	19.3	12	1.54	0.844
84	79.0	19.3	36	3.02	0.517
85	79.8	19.3	60	2.04	0.416
87	79.8	19.3	84	6.34	0.350
90	76.7	18.6	108	8.86	0.319
92	76.7	18.4	132	10.57	0.302
94	76.7	18.4	156	13.13	0.280
95	76.7	18.4	180	14.86	0.259
98	150.3	37.3	12	1.50	0.833
99	150.3	37.3	24	2.30	0.762
100	150.3	37.3	40	3.44	0.607
101	150.3	37.3	60	5.01	0.496
102	150.3	37.3	80	6.52	0.438
103	150.2	37.4	100	8.05	0.397
104	150.2	37.4	120	9.90	0.355
105	150.2	37.4	140	11.21	0.324
106	150.2	37.4	160	13.51	0.310
107	150.2	37.4	180	14.85	0.300

TABLE 2. WALL JET FRICTION FACTOR DETERMINED FROM VELOCITY PROFILES

RUN	T_∞ °F	ρ_∞ lb/ft³	x/L	U ft/sec	τ_wx10² #/ft²	Re x 10^{-3}	C_fx10³	$\frac{x}{L}Re^{-1/6}$	$C_f Re^{1/4}$x10²
66	79	0.0740	40	147.0	4.95	35.8	1.98	7.07	2.71
68	90	0.0722	60	152.0	3.46	36.5	1.33	10.6	1.83
69	78	0.0738	80	147.0	2.20	35.7	0.890	14.2	1.23
71	90	0.0722	84	152.0	2.30	36.5	0.919	14.9	1.27
73	91	0.0721	108	152.2	1.70	36.4	0.558	19.1	0.905
74	78	0.0738	120	147.0	1.40	35.7	0.609	21.2	0.830
75	81	0.0721	132	152.2	1.40	35.4	0.540	23.4	0.745
78	77	0.0740	158	146.9	1.22	35.4	0.493	28.0	0.680
79	91	0.0721	158	149.4	1.24	35.8	0.496	28.0	0.680
81	95	0.0715	180	150.0	1.02	35.5	0.408	31.9	0.559
83	87	0.0726	12	79.0	3.79	19.4	5.29	2.32	6.23
84	87	0.0726	36	79.0	1.62	19.4	2.25	6.95	2.96
85	87	0.0726	60	79.0	0.900	19.4	1.25	11.6	1.58
87	87	0.0726	84	79.8	0.614	19.4	0.844	16.2	1.01
90	87	0.0726	108	76.7	0.508	18.6	0.762	22.0	0.896
92	87	0.0726	132	76.7	0.440	18.6	0.663	25.6	0.775
94	87	0.0726	156	76.7	0.381	18.6	0.574	30.3	0.673
95	87	0.0726	180	76.7	0.316	18.6	0.477	35.0	0.558
100	77	0.0739	40	150.3	6.40	37.3	2.46	7.05	3.41
101	77	0.0739	60	150.3	4.26	37.3	1.64	10.6	2.26
102	77	0.0739	80	150.3	3.14	37.3	1.21	14.1	1.68
103	76	0.0740	100	150.2	2.43	37.3	0.937	17.6	1.30
104	76	0.0740	120	150.2	1.93	37.3	0.743	21.2	1.03
105	76	0.0740	140	150.2	1.68	37.3	0.648	24.7	0.900
106	76	0.0740	160	150.2	1.55	37.3	0.597	28.2	0.830
107	76	0.0740	180	150.2	1.32	37.3	0.508	31.7	0.707

TABLE 3. WALL JET FRICTION FACTOR

RUN	T_∞ °F	ρ_∞ lb/ft³	x/L	U ft/sec	τ_wx10² #/ft²	Re x 10^3	C_fx10³	$\frac{x}{L}Re^{-1/6}$	$C_f Re^{1/4}$x10²
61*	72	0.0749	48	102.2	2.05	25.7	1.58	8.85	2.13
				165.0	4.72	42.0	1.55	8.15	2.22
				56.1	0.66	14.0	1.80	9.78	1.97
				135.6	3.32	34.5	1.57	8.42	2.14
				96.0	2.16	7.33	1.78	10.9	1.62
				76.5	1.19	19.5	1.75	9.36	2.07
				114.6	0.75	29.0	1.80	9.48	2.11
			84	113.8	1.52	29.2	1.01	15.08	1.31
				161.0	2.90	41.0	0.935	14.2	1.33
				54.1	0.39	13.8	0.922	17.1	1.07
				221.5	5.04	56.5	0.874	13.4	1.35
				75.0	0.71	19.4	1.05	16.1	1.24
				98.4	1.18	25.0	1.05	14.5	1.30
			180	97.7	0.57	25.0	0.503	23.1	0.630
				218.1	2.44	55.6	0.440	20.1	0.575
				113.3	0.74	28.8	0.499	29.6	0.646
				161.0	1.37	41.0	0.435	30.6	0.620
				75.7	0.34	19.5	0.498	34.7	0.585
64*	79	0.0746	36	153.2	3.63	38.6	2.27	6.19	2.90
			48	153.2	4.52	38.6	1.64	8.27	2.32
			60	153.7	3.81	38.5	1.41	10.3	1.97
			84	152.1	2.59	38.1	0.964	14.2	1.35
			108	152.0	1.92	38.1	0.721	18.2	1.01
			132	152.0	1.58	38.1	0.594	22.7	0.850
			156	153.2	1.24	38.4	0.457	26.5	0.640
			180	152.0	1.19	38.1	0.443	31.0	0.620
			180	53.8	0.16	13.4	0.505	36.3	0.541
			48	53.6	0.58	13.3	1.75	9.51	1.82
			48	87.9	1.49	22.2	1.67	9.03	2.03
			48	34.8	0.24	8.17	1.71	10.05	1.62
			84	80.2	0.22	10.1	1.18	15.0	1.19
			84	87.9	0.88	22.2	0.981	15.0	1.20
70*	73	0.0744	48	41.1	0.22	10.4	1.64	10.25	1.66
			48	37.3	0.65	14.7	1.67	9.70	1.84
			24	39.1	0.56	9.86	1.15	3.17	1.14
			84	39.1	0.17	9.86	0.957	18.1	0.962
			108	39.1	0.13	9.86	0.732	23.1	0.728
			12	39.1	0.91	2.86	5.24	2.58	5.22
			24	114.6	5.09	28.6	3.38	4.33	4.32
73*	75	0.0742	36	75.1	1.67	18.1	2.61	6.99	3.03
			60	75.1	0.92	18.2	1.44	11.7	1.67
			84	75.2	0.63	18.1	0.986	16.3	1.14
			108	75.2	0.49	18.1	0.768	21.0	0.890
			132	74.6	0.41	18.0	0.653	25.0	0.736
			156	73.0	0.37	18.0	0.584	30.3	0.675
	84	0.0730	84	155.3	2.54	37.8	0.928	14.3	1.29
			108	155.3	2.19	37.6	0.800	18.7	1.11
75*	83	0.0731	48	154.0	5.17	37.5	1.92	5.33	2.67
			48	171.2	5.98	41.7	1.80	5.20	2.57
			48	123.4	3.44	30.1	1.99	5.60	2.62
	80	0.0735	24	101.0	4.19	24.7	3.60	4.44	4.51
			24	82.2	2.83	20.2	3.66	4.59	4.36
77*	82	0.0732	12	40.1	1.03	9.82	5.58	2.59	1.63
			24	40.1	0.55	9.80	3.53	5.15	1.50
			48	40.1	0.37	9.81	2.01	10.35	1.99
			60	40.0	0.28	9.75	1.54	12.95	1.53
			72	39.3	0.25	9.73	1.38	15.5	1.37
	84	0.0730	84	39.3	0.21	9.70	1.16	18.2	1.16
			108	39.7	0.16	9.64	0.893	23.4	0.886
			36	33.9	0.46	9.64	2.66	7.75	2.62
	89	0.0725	36	110.0	1.83	27.7	2.51	5.50	3.26
			36	30.1	0.29	7.30	2.82	8.12	2.60
			36	50.3	0.74	12.2	2.59	7.46	2.71
			36	70.3	1.54	16.8	2.73	7.05	3.12
	91	0.0721	36	153.7	5.31	36.2	2.01	6.36	2.78
			60	155.7	1.02	36.4	1.52	10.4	2.10
			72	155.8	3.25	36.3	1.23	12.5	1.70
	89	0.0723	84	153.4	2.60	36.6	1.07	14.5	1.48
			108	153.3	2.29	36.7	0.867	18.7	1.20
	88	0.0725	132	153.1	1.48	36.7	0.636	22.9	0.879
			156	153.2	1.39	36.8	0.527	27.0	0.726
			180	153.2	1.26	36.8	0.477	31.2	0.648
	85	0.0728	132	98.5	0.49	22.4	0.505	24.8	0.618
			132	204.5	3.27	54.3	0.572	22.4	0.872
			132	44.8	0.20	12.1	0.713	27.4	0.750
81*	85	0.0738	84	45.8	0.24	10.6	1.12	17.9	1.14
			84	98.5	0.42	14.1	1.09	17.0	1.19
			84	205.5	4.46	32.9	0.824	13.8	1.25
	89	0.0723	84	116.2	1.48	27.8	1.04	15.15	1.36
			108	116.5	1.09	27.8	0.819	19.6	1.06
			132	116.1	1.05	27.8	0.693	24.0	0.898
			156	116.6	0.86	27.8	0.562	28.2	0.725
			180	116.4	0.78	27.8	0.512	32.7	0.660
			60	116.3	2.41	27.8	1.60	10.9	2.06
			36	116.4	4.19	27.9	2.74	6.50	3.44
			12	116.6	6.45	27.9	4.20	2.18	5.45
	86	0.0725	24	116.7	5.66	28.0	1.69	4.36	4.71
			48	116.5	3.07	27.9	2.00	8.75	2.58
			72	116.5	1.96	27.9	1.28	13.0	1.65

APPENDIX: HOT-FILM ANALYSIS

An energy balance is written for the differential element shown, assuming a steady state, two-dimensional problem with conductance in the y-direction and convection in the $\tilde{x}$-direction included.

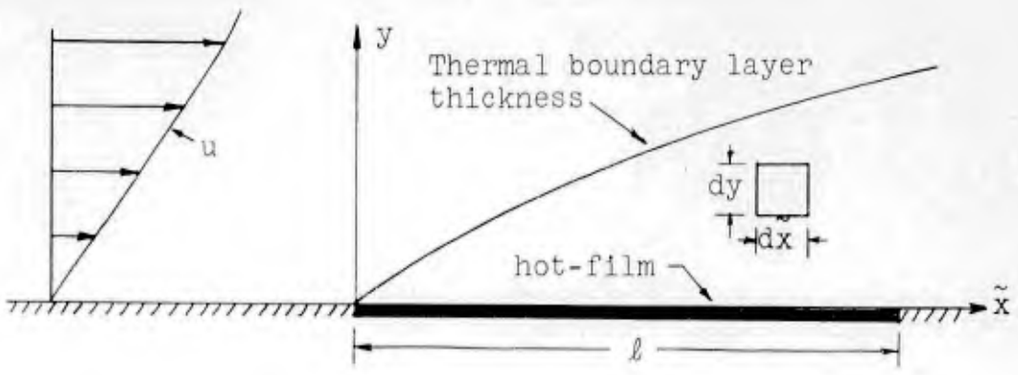

All fluid properties are assumed constant. This leads to the differential equation

$$\frac{\partial^2 T}{\partial y^2} = \frac{300\ u}{\alpha} \frac{\partial T}{\partial \tilde{x}} \tag{38}$$

Now assuming a linear velocity profile,

$$u = \frac{\alpha\beta}{300}\, y \tag{39}$$

where $\beta = 25c\tau_w g_c/k\nu$ is assumed to be constant, Eq. (38) becomes

$$\frac{\partial^2 T}{\partial y^2} = \beta y \frac{\partial T}{\partial \tilde{x}} \tag{40}$$

with the boundary conditions on $T(\tilde{x},y)$ such that $T(\tilde{x},0) = T_w$, $T(\tilde{x},\infty) = T_\infty$, and $T(0,y) = T_\infty$, where T_w is constant.

A similarity solution to Eq. (40) of the form $T = T(\sigma)$ where $\sigma = 9\tilde{x}y^n$ will be sought. When these are substituted

into (40), taking $n = -3$, the following ordinary differential equation results.

$$\frac{d^2T}{d\sigma^2} + \left(\frac{4}{3\sigma} - \frac{\beta}{\sigma^2}\right)\frac{dT}{d\sigma} = 0 \tag{41}$$

with the boundary conditions $T(0) = T_\infty$ and $T(\infty) = T_w$. Integrating (41) and applying the appropriate boundary conditions we obtain

$$\frac{T - T_\infty}{T_w - T_\infty} = 1 - \frac{\Gamma_{1/\sigma}(1/3)}{\Gamma(1/3)} \tag{42}$$

where

$$\Gamma_{1/\sigma}(1/3) = \int_0^{1/\sigma} e^{-\sigma}\sigma^{-2/3}d\sigma$$

$$\Gamma(1/3) = \int_0^{\infty} e^{-\sigma}\sigma^{-2/3}d\sigma$$

$$\sigma = \frac{9\tilde{x}}{\beta y^3}$$

The heat transfer per unit area, q'', is given by

$$q'' = -12k\left.\frac{\partial T}{\partial y}\right|_{y=0} \tag{43}$$

Differentiating (42) with respect to y and substituting into (43) we find that

$$q'' = \frac{12k(T_w - T_\infty)}{\Gamma(1/3)}\left(\frac{3\beta}{\tilde{x}}\right)^{1/3} \tag{44}$$

Then the total heat transfer, P, from a small element of width b and length ℓ is given by

$$q = \int_0^{\ell} bq''d\tilde{x} \tag{45}$$

Substituting from (44) into (45) and integrating,

$$q = \frac{3b}{2\Gamma(1/3)} \left(\frac{3\, c g_c k^2 \ell^2}{\nu} \right)^{1/3} (T_w - T_\infty) \tau_w^{1/3} \qquad (46)$$

The above equation gives a relation between the heat transfer from a hot-film and the shearing stress. This relation is the basis for the hot-film technique used in this report. Assuming constant fluid properties, we find for $T_w - T_\infty$ constant that $\tau_w \sim q^3$. The temperature distribution as a function of $\tilde{x}$ and y in Eq. (42) allows the computation of the thermal boundary layer thickness for a specified wall shearing stress as a function of the film length ℓ. This relation aids in designing a film such that the thermal boundary layer is essentially inside the laminar sublayer. The films employed to obtain the reported data were 0.020 inches wide. If this width is used to compute the thermal boundary layer thickness, it is found that ninety per cent of the temperature drop in the thermal boundary layer occurs within a y^+ of nine at the worst operating conditions. Since the wall jet flow was shown to be similar to the flat plate flow used in calibrating out to y^+ of about thirty (Fig. 11), and since the layers close to the wall are of the greatest importance in the heat transfer, the films employed were adequate for the determination of the shearing stress.

UNCLASSIFIED